UAL/ETEAPOT Benchmark Comparisons V: Spin Evolution in an All-Electric Lattice Coasting Beam—Preliminary

J. D. Talman and R. M. Talman

July 10, 2014

Abstract

The main purpose for this report is to document the treatment of spin evolution by UAL/ETEAPOT. By this time ETEAPOT supports bunched beam spin evolution but, for this report, there is no RF cavity and no synchrotron oscillations. With no RF cavity in the ring, only coasting, not bunched, beams can be modeled. Since long spin correlation time (SCT) can only be achieved with bunched beams, the tracking described here can determine parameters affecting SCT but cannot obtain usefully long SCT values directly. Direct determination of bunched beam SCT values using ETEAPOT will be the subject for a "Benchmark Comparisons-VI" report.

For the present report, a new lattice called `E_Protonium.sxf` (with $m = 0$ and $m = 1$ variants) is introduced and tracked. "m=1 protonium" is a hypothetical atom consisting of a single proton bound to an infinite mass charged particle at the origin; the charge is just right so that a proton having the magic frozen spin momentum can travel in a circle of radius $r_0 = 40\,\mathrm{m}$, which is the radius of the nominal proton EDM lattice. "m=0 protonium" is the same except the central charge is a fixed line charge of the correct strength for magic momentum protons to be bound in a circle of the same $r_0 = 40\,\mathrm{m}$ radius.

There is no pretense that "protonium" is a physically useful or even realizable atom, nor is there pretense that the lattice can serve as a practical EDM apparatus. Though structured with a large number of (identical) bending elements, all drift lengths are set nearly to zero. What is left is a physical system all of whose parameters, in particular SCT, can be calculated analytically, with orbits close to the design orbit treated perturbatively. This provides the simplest possible configuration for testing the reliability of the code and for comparison with other codes.

The "physics" emphasis in this report is on comparing $m = 1$ and $m = 0$ spin evolution. One significant observation is a four orders of magnitude greater spin decoherence with $m = 1$ than with $m = 0$, admittedly in a special case. More surprising is the observation that orbits "damp" to perfect circles. It is not known at present whether this settling to perfect circles (suspicious for a Hamiltonian system) is valid or is a spurious numerical artifact, occurring, for example, in the artificially-included quadrupoles or straight sections. If the settling to perfect circles is valid, it is especially important for the m=0, cylindrical case since SCT is then almost arbitrarily large; this is referred to here as *the cylindrical miracle*. Since the settling to perfect circles occurs within hundreds of turns, the result can be checked independently, for example by Runge-Kutta tracking.

Contents

1 Tracking Results and Interpretation

1.1 Introduction

The initial part of this report contains ETEAPOT spin tracking results and tentative explanation of them. Lengthier and more technical documentation of the code is contained in appendicies. Only two lattices are analysed and both are highly idealized, primarily by having bends separated only by negligibly short straight sections and by having extremely weak quadrupoles, just strong enough for betatron motion in both planes to be stable. One lattice is "cylindrical" or $m = 0$, the other is "spherical" or $m = 1$. To encourage the reader to think of an electric accelerator storage ring as not essentially different from an atom, these lattices are referred to as two variants of a hypothetical atom called "protonium", with a single proton bound to a fixed line charge or point charge.

1.2 Parameters and Twiss Functions of the "Protonium" Lattices

Table 1: For m=1 the force field is central, which makes the design orbit degenerate—every circular orbit with the design energy is effectively an equatorial orbit. This causes Q_y in the m=1 case to be ambiguous; with the design orbit *defined* to lie in the horizontal plane, a particle with initial vertical offset is interpreted as having Q_y=1, in spite of the fact that its orbit lies in a single (slanted) plane, and is congruent to the design orbit. For the m=0, cylindrical case, tiny vertically focusing quads of strength q, are inserted to restore marginal stability. The source of the "indeterminate" entry in one case is a nuisance associated with inverse trig functions, with vertical tune extremely small and vertical beta function extremely large. Otherwise there is excellent agreement between two independent codes conserning the standard lattice functions.

file name	variable name	unit	m=0, cylindrical	m=1, spherical
cells/arc	`NCellPerArc`		20	20
bend radius	`r0`	m	40.0	40.0
half drift length	`Ldh`	m	10^{-6}	10^{-6}
half bend per cell	`Thetah`	r	0.078539816	0.078539816
half bend length	`Leh`	m	3.141592	3.141592
circumference	`circum`	m	251.327	251.327
inv. focal length	`q`	1/m	1.0e-6	1.0e-6(effective)
field index	`m`		0.0	1.0
horz. beta(MAPLE)	`betax`	m	31.24	49.92
horz. beta(ETEAPOT)		m	31.19	49.92
vert. beta(MAPLE)	`betay`	m	1772	40.00
vert. beta(ETEAPOT)		m	1765	indeterminate
horz. tune(MAPLE)	`Qx`		1.2813	0.8012
horz. tune(ETEAPOT)			1.2815	0.8012
vert. tune(MAPLE)	`Qy`		0.0225	1.0000
vert. tune(ETEAPOT)			0.0226	1.0000

1.3 Simplifications

This report documents spin evolution of polarized protons as predicted by ETEAPOT. It is preliminary and over-simplified in two ways compared to the spin tracking that will eventually be required for the proton EDM measurement.

One oversimplification is the restriction to coasting beams—with no RF cavitities there is no longitudinal acceleration and any spread of injection energy will cause the coasting beam to spread longitudinally. Spin coherence times (SCT) obtained this way are expected to be far too short to permit realistic EDM

measurements; it is only with synchrotron oscillation averaging that acceptably long SCT values can be expected. The purpose for the present preliminary tracking is to quantify the SCT contributions due to various initial phase space offsets from the design orbit.

The other simplification is that the lattice will be "all bends" with no straight sections. In numerical treatments like ETEAPOT, the presence of absence of straight sections is of little consequence. But for analytic precession calculations the presence of straight sections provides undesirable complication. To better motivate analytic calculations, and as a mnemonic, we refer to the drift-free lattice as "protonium". Analytic treatment of the protonium atom can then be compared with numerical treatment of the same system treated as an accelerator lattice.

1.4 Cautionary Comments

The drift lengths in the `E_Protonium.sxf` lattice are negligibly short compared to electrode separation "*gap*". This is opposite to the usual situation, in which drift lengths are long compared to fringe field lengths, which is what ETEAPOT assumes by default. So, for investigating protonium, the fringe field correction has to be set to zero in the code.

In this report, the contributions to spin precession for various initial phase space displacements differing from zero are obtained. All six coordinates are treated on equal terms. This is misleading as regards interpretation of the relative importance of transverse and longitudinal initial offsets. Nevertheless, ignoring this distinction, reading from plots shown later, entries are made in Table 2, and interpreted as spin coherence times due to the various offsets.

Table 2: Excess precession caused by various initial phase space conditions for the particles being tracked. The entries are obtained from Figures 1 through 4. One notes that all SCT values in the table are very short compared to the nominal target value of SCT=1000 s desired for the proton EDM experiment. But the results shown here are for coasting beams; for bunched beams there will be energy averaging accompanying synchrotron oscillations that can be expected to increase the SCT values by, perhaps, two orders of magnitude. Excess precession for examples in the first six rows are expected to be quadratic in initial coordinate offset. Only for the final two rows are the excess precessions expected to be linear in the initial coordinate offset. The only surprise in this table is the dramatic difference between SCT values due to energy offset in the cylindrical and spherical cases; i.e. the two bottom rows. This is discussed in a later "Cylindrical Miracle" section.

initial offsets	Δs_x/turn[Z]	SCT[Z] "cylindrical" s	Δs_x/turn[P1.0]	SCT[P1.0] "spherical" s
0.0005 0 0 0 0 0	-1.1e-7	9	-1.5e-7	7
-0.0005 0 0 0 0 0	-1.1e-7	9	-1.5e-7	7
0 0.0002 0 0 0 0	-1.6e-7	6	-6.3e-7	1.6
0 -0.0002 0 0 0 0	-1.6e-7	6	-6.3e-7	1.6
0 0 0.01 0 0 0	1.8e-7	5.5	2.5e-7	0.4
0 0 0 0.01 0	N/A	N/A	4.1e-6	0.24
0.01 0 0 0 0 5.85e-5	-4.8e-7	2.1	1.4e-3	0.0007
0 0 0 0 0 5.85e-5	-4.6e-7	2.2	1.4e-3	0.0007

By up-down symmetry, the excess precession Δs_x/turn has no contribution proportional to either y_0 or y'_0. The leading vertically-induced decoherence is proportional to $\epsilon_{y,CS}$, the (generalized) vertical Courant-Snyder invariant, which is quadratic in y_0 and y'_0. Horizontal betatron oscillations are similarly proportional to the horizontal invariant $\epsilon_{x,CS}$ (though there is also the possibility of contributions depending on x_0 or x'_0 multiplied by energy offset $\Delta\mathcal{E}$). But decoherence due to initial energy offset $\Delta\mathcal{E}$ is different. There will be excess precession linear in $\Delta\mathcal{E}$. In spite of these differences, for semi-quantitative comparison in Table 2, because all 8 particles have "typical" amplitudes, their contributions to SCT are simply quoted as the excess precession per turn divided by the time per turn.

1.5 Protonium

As introduced in the abstract, "protonium" is an imaginary atom formed from a single proton bound to a fixed (i.e. infinite mass) negative point charge situated at the origin. With the proton anomalous magnetic moment being $G = 1.79284736$, the magic momentum is $p_0c = 0.7007405364\,\mathrm{GeV}$, the velocity is $0.5983790769c$ and radial electric field E_m required to give a circular orbit of radius $r_0 = 40\,\mathrm{m}$ is

$$E_m = \frac{(m\gamma_0 v/e)\beta_0 c}{r_0} = \frac{(p_0 c/e)\beta_0 c}{r_0} = 0.0104827119\,\mathrm{GV/m}. \tag{1}$$

The charge $Q_{m=1}$ giving this electric field at distance r_0 is

$$Q_{m=1} = 4\pi\epsilon_0 r_0^2 E_m = 1.866174\,\mathrm{C}. \tag{2}$$

The corresponding line charge density $\lambda_{m=0}$ for $m = 0$ is

$$\lambda_{m=1} = 2\pi\epsilon_0 r_0 E_m = 0.023327180\,\mathrm{C/m}. \tag{3}$$

To produce orbits close to the design circular orbit, ETEAPOT treats the protonium as an accelerator lattice consisting of a large number (such as 80 elements, each bending through $2\pi/80$) separated by straight sections of negligible length.

One possible source of confusion is that particle energies in ETEAPOT are established *outside* bend elements. This continues to be true for protonium, even though the particles are almost never outside bend elements. Bend elements are treated as having "hard" edges, meaning the electric potential changes discontinuously from zero outside, to non-zero inside. The drift lengths, though short, e.g. 1 micrometer, are not exactly zero. Particle energies are assigned, and subsequently evaluated, within the drift sections. Of course the total particle energy, mechanical (rest energy plus kinetic energy) plus potential is conserved (except in RF cavities of which there are none at present), so the discontinuous change of potential energy causes a cancelling change in kinetic energy. For straight sections of negligible length the net fringe field effect as a particle proceeds from just before exiting a bend element to just after entering the next one can be neglected.

2 Coasting Beam Spin Precession in Idealized Rings

2.1 Spin Evolution

The following series of figures compare spin evolution (actually just the transverse spin component $s_x \equiv s[0]$) for various particles all having initial spin purely longitudinal (where "longitudinal means "along the tangent to the design orbit" *not* "along the particle's orbit".

Initial phase space coordinates are indicated at the top of each graph in the form `Z(or P1.0): x_0, x'_o, y_0, y'_0, ct_0, dE_0/(p_0c)`, where `Z` stands for $m = 0$, "cylindrical" electrodes, and `P1.0` stands for $m = 1.0$, "spherical" electrodes. Very weak vertically focusing quads, of strength q given in the parameter table, provide just enough vertical focusing so that orbits are stable vertically. With weak vertical focusing the $m = 0$ case is barely stable vertically, causing particles with too great vertical momenentum to be lost.

Hint concerning running the code: Initial conditions for the 21 (or any other number of particles being tracked) are given in the `userBunch` file, an example of which is given in an appendix.

The graphs of Figure 1 indicate that the spin precession accompanying initial horizontal displacement depends only weakly on the value of m. The graphs of Figure 2 show the precession accompanying initial horizontal slope somewhat greater with m=1 than with m=0.

The graphs may seem, superficially, to contradict the assumption that the spins are purely longitudinal initially. But betatron oscillations rapidly produce small transverse spin components of the same order as the betatron slope components.

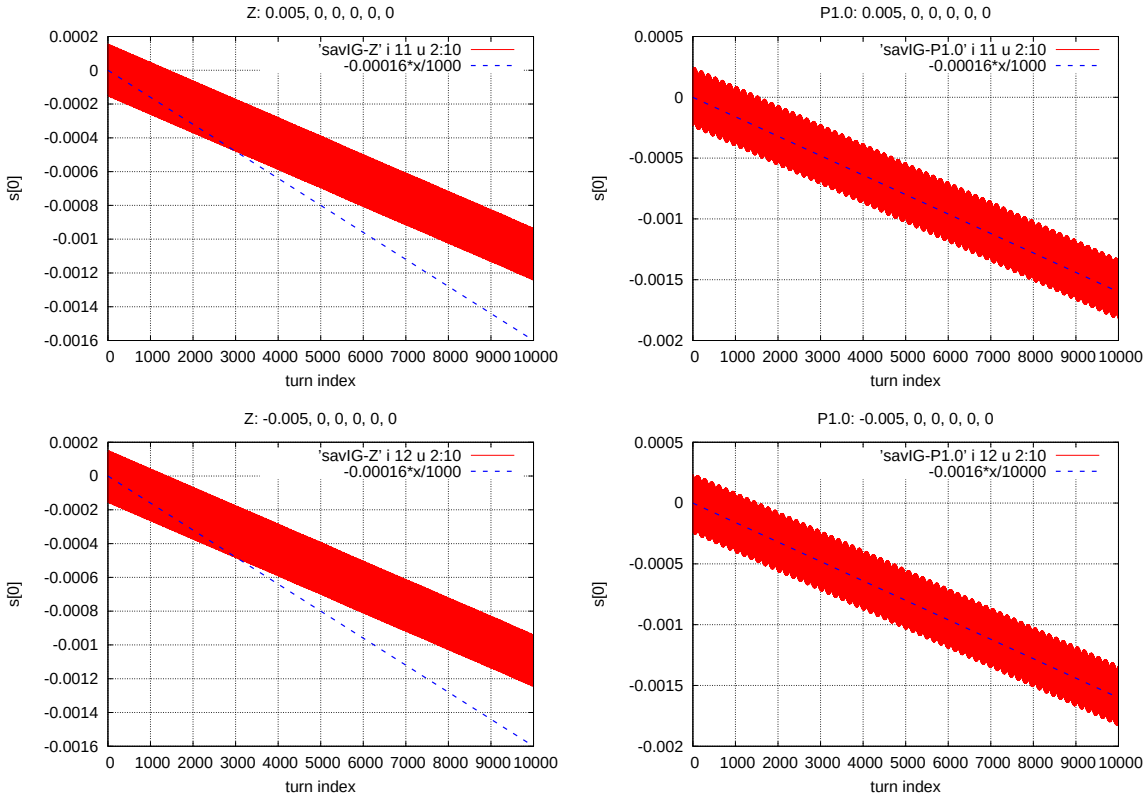

Figure 1: The figures on the left have $m = 0$, those on the right have $m = 1$. The upper/lower figures have initial horizontal displacements $x_0 = \pm 5\,\mathrm{mm}$, and all other initial displacements zero. The dashed lines are fits to the right graph copied to the left.

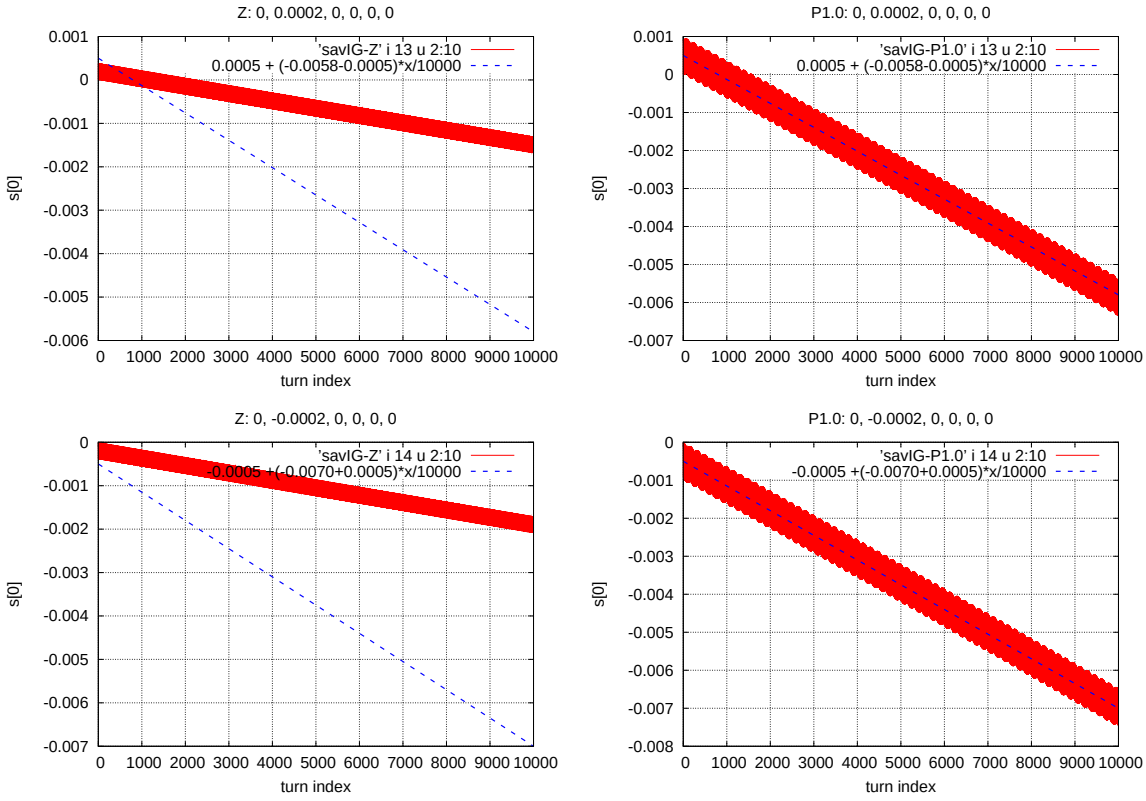

Figure 2: The figures on the left have $m = 0$, those on the right have $m = 1$. The upper/lower figures have initial horizontal slopes $x_0' = \pm 0.0002$, and all other initial displacements zero. The dashed lines are fits to the right graph copied to the left.

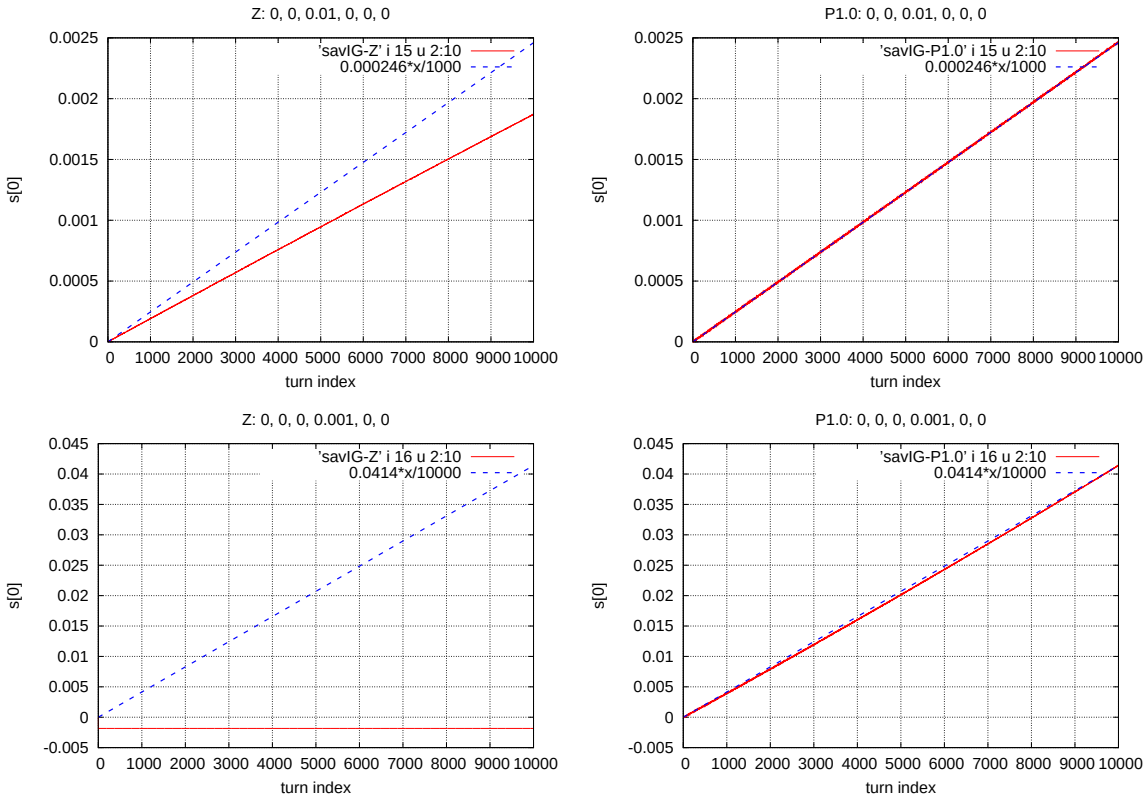

Figure 3: The figures on the left have $m = 0$, those on the right have $m = 1$. The upper figures have initial vertical displacement $y_0 = 0.01$, and all other initial displacements zero. The lower figures have initial vertical slope $y_0' = 0.001$, and all other initial displacements zero. The dashed lines are fits to the right graph copied to the left. (Because there is no vertical focusing in the $m = 1$ case, the vertical displacement rapidly increases beyond the ETEAPOT default aperture of 1 m in *the lower left graph, which therefore has to be ignored.*)

Figure 3 shows dependence on initial vertical displacements and slopes. For consistency there is the same up/down and left/right graph organization of graphs. But the lower left graph has to be ignored because the $m = 0$ lattice is insufficiently stable vertically. By default treatment in ETEAPOT, particle transverse positions are not allowed to exceed 1 meter; this occurs after just a few turns with the initial vertical slope being 0.001.

Figure 4 shows dependence on initial energy offset, for two initial radial offsets. Again, the graphs on the left are for cylindrical, on the right for spherical. The excess precessions in the m=1 spherical case are so great that the spin makes about three complete revolutions relative to the particle momentum during the 10,000 turns shown; this is shown by the sinusoidal variation of s_x between +1 and -1. Yet the excess precession for a particle with the same initial conditions is barely visible in the m=0 cylindrical case.

This four order of magnitude difference in excess precession is, by far, the most striking observation in the report—enough so to be discussed further in the subsequent "cylindrical miracle" section.

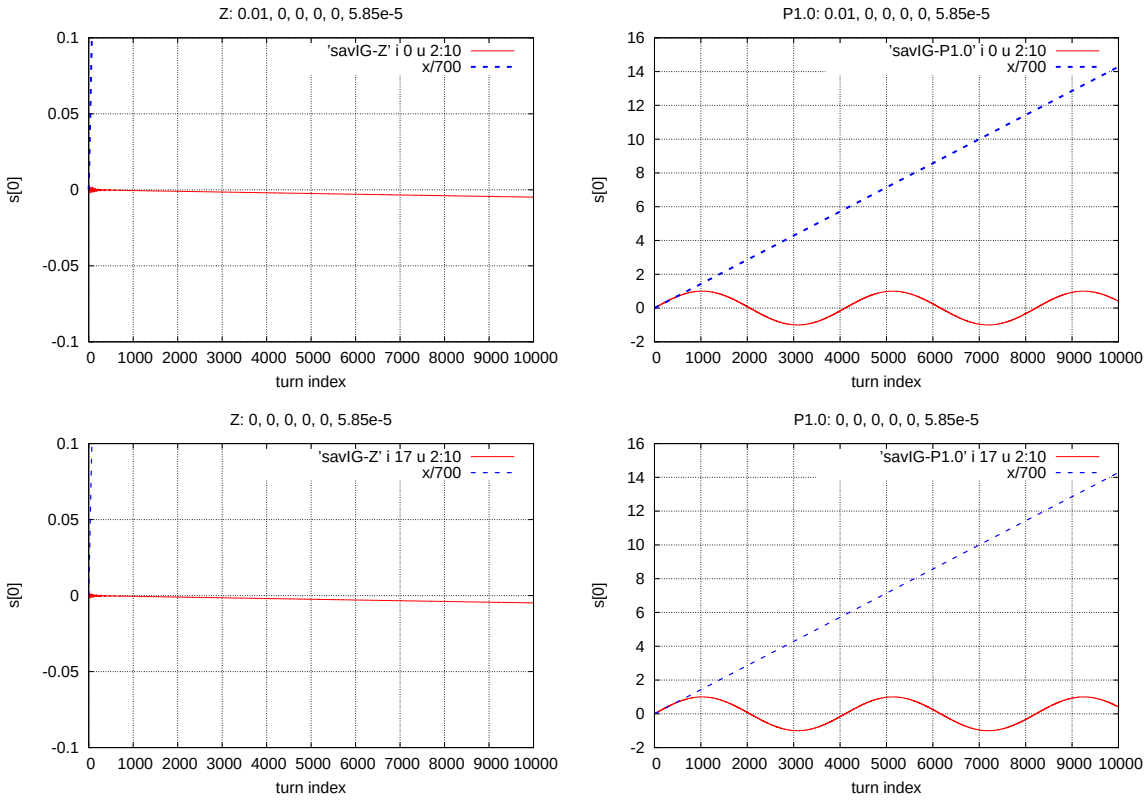

Figure 4: The figures on the left have $m = 0$, those on the right have $m = 1$. The upper figures have initial horizontal displacement 1 cm and (normalized) off-energy displacement 5.85e-5; these displacements are matched to cause the subsequent orbit to be exactly a circle of radius 1 cm greater than the design orbit in the $m = 1$ protonium case (but not in the $m = 0$ cylindrical case). The lower figure has the same energy offset but vanishing initial horizontal displacement. The dashed lines are fits to the right graph copied to the left. Note that the precession rate is so much greater for the m=1 (spherical) case, than for the m=0 (cylindrical) that the dashed lines are just barely visible in plots on the left, even with the vertical range so great that the precession in the $m = 0$ case is itself barely visible. All by themselves these plots make the case for the superiority of m=0 over m=1 for long spin coherence time.

2.2 The "Cylindrical Miracle"

The particular choice of initial conditions; $(x_0, x_0', y_0, y_0', ct_0, \mathcal{E}/(p_0c)) = (0.01, 0, 0, 0, 0, 5.85e\text{-}5)$ was not arbitrary. Rather, the value $\mathcal{E}/(p_0c) = 5.85\text{e-}5$ is exactly the energy offset for which a particle will travel exactly in a circle of radius 40.01 m in the m=1 spherical lattice. This corresponds to a calculable offset $\Delta\gamma = \gamma - \gamma_0$ relative to the magic (or design) value γ_0. This behavior is confirmed by ETEAPOT, in the upper right graph of Figure 5. Then, because the velocity is permanently offset by an appreciable amount, it is not surprising that the excess spin precession is large (i.e. three complete revolutions in 10,000 turns). The initial energy offset was not exactly correct but, noting the exceedingly expanded scale, it was close. One notes, though, a bit of fuzziness near the start, which is therefore blown up in the lower right figure.

Initial oscillations are not the most striking feature of the lower right figure. With the initial energy offset not quite correct, one expects the particle to execute tiny perpetual oscillations about a value close to the intended value of $x = 0.01\,\text{m}$. In fact, the particle quickly "damps" to *exactly* a circle of radius 40.01006 m. Here "damp" is in quotation marks, since there can be no true damping in a Hamiltonian system. But can there not be rapid sloshing of energy from one form, potential, to another, kinetic? Certainly there can, but whether the "action" can decay remains to be investigated. A more mundane explanation might be that the damping is a spurious artifact of the particle tracking. Certainly it is not unusual for errors in numerical treatment to introduce "friction" that causes shrinkage or growth of oscillations.

Without pretending to understand whether or not the damping is spurious, we proceed to observe, in the upper left figure, the momentum evolution of the same particle in the $m = 0$, cylindrical lattice. Instead of exhibiting perpetual synchrotron oscillations about some appropriate off-momentum closed orbit, the particle again "damps" onto an off-momentum closed orbit. Furthermore this orbit is seen (because $x = 0.004\,\text{m}$ for ever) to be a circle (which it obviously has to be, given the simplicity of the system). All that is left is to apply conservation of energy, along with the known dispersion in the $m = 0$ lattice, to check that the particle should indeed settle to $x = 0.004\,\text{m}$, and then to figure out what its excess spin precession should then be. Actually it is simpler than this, because we know that *all circular orbits* in the cylindrical case have the magic velocity. Therefore, if a particle indeed settles to a circular orbit, its velocity is necessarily magic, it has no excess precession, and its SCT value is infinite. **This is the Cylindrical Miracle.**

Even if the settling to perfect circles is spurious the true orbits undoubtedly oscillate about the circle on which the speed is magic. This causes the spin decoherence to be at least close to zero in the $m = 0$ case. This reduces the urgency of finding whether or not the settling to perfect circles is valid.

However there is another issue making it important to know the true nature of the orbits. Use of the m=0, cylindrical lattice is thought to be contra-indicated by intrabeam scattering (IBS). If, however, the radial beam temperature (like the vertical beam temperature) is extremely low, as could be the case with purely circular orbits, the intrabeam scattering might be greatly reduced. By running at low RF frequency and amplitude, the bunch lengths can be very long, which also helps to reduce IBS.

Even in the most optimistic scenario, with all orbits being perfect circles (actually gentle helices) the injection acceptance into the cylindrical lattice is extremely small, which obviously limits the number of protons that can be stored.

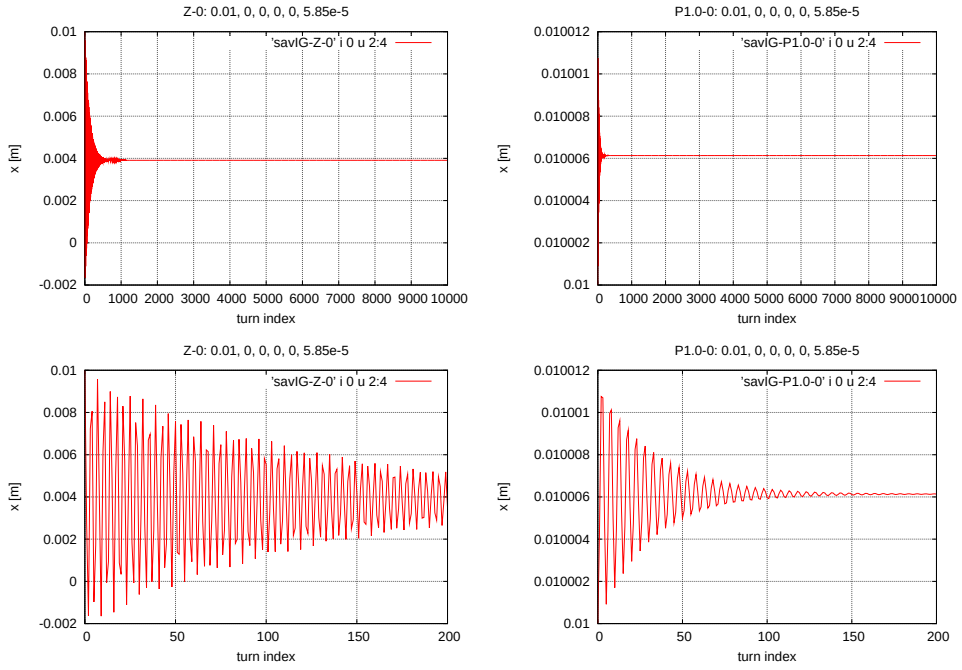

Figure 5: In these plots radial displacements x are plotted against turn number. The lower plots zoom in on the first 200 turns. As in previous figures the m=0, cylindrical plots are on the left, the m=1, spherical plots are on the right.

A Spin Tracking in ETEAPOT

A.1 Approximations

- To leading approximation all spin precession occurs in central force, inverse square law, "Kepler force" regions. With this assumption the orbit through a bend element of any individual particle lies in a single fixed plane.
- Each individual particle's spin vector can be decomposed into a (conserved) component $\tilde{s}_\perp$, normal to the bend plane, and a (precessing) 2-component vector $\tilde{\mathbf{s}}_\parallel$, lying in the bend plane.
- Initially hard edge bends are assumed. Even after this approximation is dropped it will be assumed that the paths through the entrance and exit fringe fields continue to lie in the same plane as in the bend interior.
- As always in ETEAPOT, field deviations from "Spherical" will be modeled by artificial quadrupoles.
- Quadrupoles, whether real or artificial (and all multipoles) will be treated as thin. Spin evolution through multipoles will be modeled by successive rotations. All such rotations will be concatenated explicitly into a single (near-identity) precession matrix. This will circumvent the problem of large, approximately canceling precessions and avoid spurious non-commutative geometric precessions.
- Quadrupoles too thick to be validly treated as thin, will be sliced, with regions between the sliced thin quadrupoles treated as drifts.
- Bend frame spin components are $(\tilde{s}_x, \tilde{s}_y, \tilde{s}_z)$, laboratory frame spin components are (s_x, s_y, s_z).

A.2 Spin Coordinates

A.2.1 Bend Coordinates

For studying spin evolution in a frozen spin storage ring we use the coordinate system shown in Figure 6. The local frame of reference is the Frenet frame aligned with the orbit of the individual particle being tracked, with $\mathbf{e_1}$ pointing in the centrifugal (outward) direction, $\mathbf{e_3}$ pointing in the tangential direction and $\mathbf{e_2}$ pointing out of the page.

The figure shows the angle $\tilde{\alpha}$ which is the angle in the bend plane between the projection of the spin vector onto the bend plane and $\mathbf{e_3}$, tangent to the particle orbit. Spin precession is most naturally described by using, as spin coordinates, the angle $\tilde{\alpha}$ and $\tilde{s}_y$, the vertical component of spin in the bend frame. Though the spin vector has three components, only two are independent; the angle $\tilde{\alpha}$ fixes the direction of $\tilde{\mathbf{s}}_\parallel$ in the bend plane. The spin precesses about the $\tilde{y}$-axis in the bend plane. The bend frame spin coordinates are

$$\begin{pmatrix} \tilde{s}_x \\ \tilde{s}_y \\ \tilde{s}_z \end{pmatrix} = \begin{pmatrix} -\tilde{s}_\parallel \sin\tilde{\alpha} \\ \tilde{s}_\perp \\ \tilde{s}_\parallel \cos\tilde{\alpha} \end{pmatrix}. \tag{4}$$

Only two coordinates are necessary because the magnitude of $\tilde{\mathbf{s}}$ is equal to 1;

$$\tilde{s}_\parallel^2 + \tilde{s}_\perp^2 = 1. \tag{5}$$

(Note that $\tilde{\mathbf{s}}_\parallel$ is the 2D vector component of the spin vector in the bend plane, *not* the component of the spin vector parallel to the velocity.) These coordinates are ideal for evolving the spins through ring elements which cause horizontal bends.

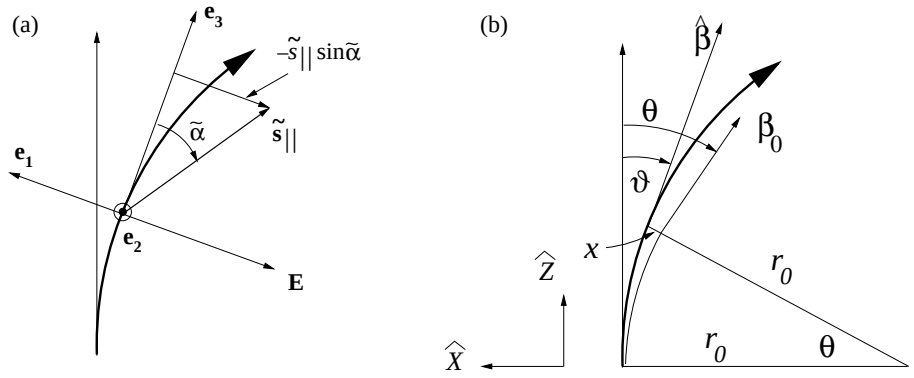

Figure 6: (a) In the bend plane the spin vector $\mathbf{s}$ has precessed through angle $\tilde{\alpha}$ away from its nominal direction along the proton's velocity. (Remember that different particles have different bend planes.) (b) Projection of figure (a) onto the laboratory horizontal plane. The projected longitudinal axis is shown coinciding with the laboratory longitudinal axis, even if this is not exactly valid. x is the deviation of the (bold face) particle orbit from the (pale face) design orbit. If the bend plane coincides with the design bend plane (as is always approximately the case) $\hat{\boldsymbol{\beta}}_0$ and $\hat{\mathbf{z}}$ are identical. θ is the reference particle deviation angle from longitudinal and ϑ is the tracked particle deviation angle from longitudinal. On the average θ and ϑ are the same, but betatron oscillations cause them to differ on a turn by turn basis, and also to make the instantaneous bend plane not quite horizontal.

A.2.2 Transformation From Lab Frame to Bend Frame

From the particle tracking one has the laboratory frame vectors $\mathbf{r}$, $\mathbf{p}$, and hence $\mathbf{L} = \mathbf{r} \times \mathbf{p}$, just past the bend entrance, and one also has the spin vector $\mathbf{s}$;

$$\begin{aligned}
\mathbf{r} &= r_x\hat{\mathbf{x}} + r_y\hat{\mathbf{y}} + r_z\hat{\mathbf{z}}, \\
\mathbf{p} &= p_x\hat{\mathbf{x}} + p_y\hat{\mathbf{y}} + p_z\hat{\mathbf{z}}, \\
\mathbf{L} &= L_x\hat{\mathbf{x}} + L_y\hat{\mathbf{y}} + L_z\hat{\mathbf{z}}, \\
\mathbf{s} &= s_x\hat{\mathbf{x}} + s_y\hat{\mathbf{y}} + s_z\hat{\mathbf{z}}.
\end{aligned} \tag{6}$$

We can establish an orthonormal, right-handed basis triad with axis 3 parallel to $\mathbf{p}$ and axis 2 parallel to $-\mathbf{L}$ (where the negative sign is appropriate for clockwise orbits);

$$\begin{aligned}
\mathbf{e_3} &= \frac{p_x}{p}\,\hat{\mathbf{x}} + \frac{p_y}{p}\,\hat{\mathbf{y}} + \frac{p_z}{p}\,\hat{\mathbf{z}}, \\
\mathbf{e_2} &= \frac{\mathbf{r}\times\mathbf{p}}{-L}, \\
\mathbf{e_1} &= \mathbf{e_2}\times\mathbf{e_3}.
\end{aligned} \tag{7}$$

These equations can be re-expressed formally, with all coefficients known, as

$$\begin{aligned}
\mathbf{e_1} &= a_{11}\hat{\mathbf{x}} + a_{12}\hat{\mathbf{y}} + a_{13}\hat{\mathbf{z}} \\
\mathbf{e_2} &= a_{21}\hat{\mathbf{x}} + a_{22}\hat{\mathbf{y}} + a_{23}\hat{\mathbf{z}} \\
\mathbf{e_3} &= a_{31}\hat{\mathbf{x}} + a_{32}\hat{\mathbf{y}} + a_{33}\hat{\mathbf{z}}.
\end{aligned} \tag{8}$$

The vector $\mathbf{s}$ can be expanded as

$$\begin{aligned}
\mathbf{s} &= \tilde{s}_1\mathbf{e_1} + \tilde{s}_2\mathbf{e_2} + \tilde{s}_3\mathbf{e_3} \\
&= \tilde{s}_1(a_{11}\hat{\mathbf{x}} + a_{12}\hat{\mathbf{y}} + a_{13}\hat{\mathbf{z}}) + \ldots \\
&= (a_{11}\tilde{s}_1 + a_{21}\tilde{s}_2 + a_{31}\tilde{s}_3)\,\hat{\mathbf{x}} + \ldots .
\end{aligned} \tag{9}$$

The final relation can be expressed in matrix form as

$$\begin{pmatrix} s_x \\ s_y \\ s_z \end{pmatrix} = \mathbf{R} \begin{pmatrix} \tilde{s}_1 \\ \tilde{s}_2 \\ \tilde{s}_3 \end{pmatrix}, \tag{10}$$

where $\mathbf{R}$ is an orthogonal matrix,

$$\mathbf{R} = \begin{pmatrix} a_{11} & a_{21} & a_{31} \\ a_{12} & a_{22} & a_{32} \\ a_{13} & a_{23} & a_{33} \end{pmatrix}. \tag{11}$$

(Aside: the magnitude $|\det\mathbf{R}|$ of the determinant of $\mathbf{R}$ is necessarily 1, but the actual value is ± 1. This sign correlates with the clockwise/counterclockwise orbit ambiguity.)

Because $\mathbf{R}$ is orthogonal, $\mathbf{R}^{-1} = \mathbf{R}^T$ and Eq. (10) can be inverted to give

$$\begin{pmatrix} \tilde{s}_1 \\ \tilde{s}_2 \\ \tilde{s}_3 \end{pmatrix} = \begin{pmatrix} a_{11} & a_{12} & a_{13} \\ a_{21} & a_{22} & a_{23} \\ a_{31} & a_{32} & a_{33} \end{pmatrix} \begin{pmatrix} s_x \\ s_y \\ s_z \end{pmatrix}. \tag{12}$$

This yields the spin components in the bend frame. Their propagation through the bend is described below. At the exit of the bend element the laboratory-frame components can be worked out using a similar formula.

A.2.3 Non-Bend Elements

Some elements (especially quadrupoles) can cause vertical deflections which alter s_y. Being proportional to transverse displacements these deflections are very small and can have either polarity. Nevertheless it is necessary to keep track of their effects.

On an element by element basis, when a particle has just entered an element that bends (for example) in a plane rolled counter-clockwise by angle ϕ about the z-axis, it is first necessary to transform its laboratory frame coordinates (s_x, s_y, s_z) into bend frame coordinates $(\tilde{s}_x, \tilde{s}_y, \tilde{s}_z)$ using

$$\begin{pmatrix} \tilde{s}_x \\ \tilde{s}_y \\ \tilde{s}_z \end{pmatrix} = \begin{pmatrix} \cos\phi & -\sin\phi & 0 \\ \sin\phi & \cos\phi & 0 \\ 0 & 0 & 1 \end{pmatrix} \begin{pmatrix} s_x \\ s_y \\ s_z \end{pmatrix} \tag{13}$$

(As it stands, this equation is over-simplified since (in the presence of vertical betatron oscillation) the normal to the bend plane can have a (tiny) component along the longitudinal axis. This complication is temporarily being ignored.) The roll angle ϕ has been chosen so that the element causes pure precession through some calculable angle $\widetilde{\Delta\alpha}$ about some known axis. With the particle speed known, $\widetilde{\Delta\alpha}$ is determined unambiguously by the (known) magnitude of the angular deflection in the multipole element. The plane of deflection is also available from the particle tracking through the element. Expressing the spin precession also by a 3×3 matrix, and transforming back to the erect laboratory frame, one obtains the new cartesian components,

$$\begin{pmatrix} s_x \\ s_y \\ s_z \end{pmatrix}_{\text{after}} = \begin{pmatrix} \cos\phi & \sin\phi & 0 \\ -\sin\phi & \cos\phi & 0 \\ 0 & 0 & 1 \end{pmatrix} \begin{pmatrix} \cos\widetilde{\Delta\alpha} & 0 & -\sin\widetilde{\Delta\alpha} \\ 0 & 1 & 0 \\ \sin\widetilde{\Delta\alpha} & 0 & \cos\widetilde{\Delta\alpha} \end{pmatrix} \begin{pmatrix} \cos\phi & -\sin\phi & 0 \\ \sin\phi & \cos\phi & 0 \\ 0 & 0 & 1 \end{pmatrix} \begin{pmatrix} s_x \\ s_y \\ s_z \end{pmatrix}_{\text{before}} \tag{14}$$

As mentioned earlier, matrix products like these are to be explicitly concatenated, outside ETEAPOT, with all elements expressed as (rapidly convergent) truncated expansions in products of (small) angles and (small) precession angle $\widetilde{\Delta\alpha}$. The resultant matrix (coded into ETEAPOT) differs from the identity matrix only by differentially-small, rapidly-convergent elements.

A.3 Spin Evolution Through Muñoz-Pavic Bends

A.3.1 Analytic Formulas for Spin Precession

We introduce, at least temporarily, the term "Muñoz-Pavic Bend" to characterize a bend having field index $m = 1$, which is the case being treated in our 2D formalism. In this case (and only in this case) the orbit stays in a single plane. Also, in this frame any precession of the spin is purely around an axis normal to the plane. Obtaining the initial values of the spin components in this frame was described in the previous section.

In the bend plane the orbit lies in a single plane. Superficially this may suggest we are accounting only for horizontal betatron oscillations and neglecting vertical betatron oscillations. In fact, however, the ETEAPOT treatment accounts for arbitrary betatron and synchrotron motion by assigning different "wobbling planes" to each individual particle. Even allowing for vertical betatron motion these frames are all very nearly parallel to the global horizontal design frame of the ring. For the 2D evolution through electric bend elements in ETEAPOT, any betatron oscillations actually present for a particular particle are folded into the determination of its particle-specific orbit plane, and the initial coordinates in this plane.

As shown in Figure 6, the initial spin vector is

$$\tilde{\mathbf{s}} = -\tilde{s}_{\parallel} \sin\tilde{\alpha}\,\hat{\mathbf{x}} + \tilde{s}_y\hat{\mathbf{y}} + \tilde{s}_{\parallel}\cos\tilde{\alpha}\,\hat{\mathbf{z}}. \tag{15}$$

Here $\tilde{s}_y\hat{\mathbf{y}}$ is the out-of-plane component of $\tilde{\mathbf{s}}$, $\tilde{s}_{\parallel}$ is the magnitude of the in-plane projection of $\tilde{\mathbf{s}}$, and $\tilde{\alpha}$ is the angle between the projection of $\tilde{\mathbf{s}}$ onto the plane and the tangent vector to the orbit.

Jackson's[12] Eq. (11.171) gives the rate of change in an electric field $\mathbf{E}$, of the longitudinal spin component as

$$\frac{d}{dt}\,(\hat{\beta}\cdot\mathbf{s}) = -\frac{e}{m_p c}\,(\mathbf{s}_{\perp,\mathbf{J}}\cdot\mathbf{E})\left(\frac{g\beta}{2} - \frac{1}{\beta}\right). \tag{16}$$

(Note that Jackson's $\mathbf{s}_{\perp,J}$ is the component perpendicular to the tangent to the orbit *not* to the orbit plane.) Substituting from Eq. (15) the equation becomes

$$\frac{d}{dt}\,(\tilde{s}_{\parallel}\cos\tilde{\alpha}) = -\frac{e}{m_p c}\,(\tilde{s}_{\parallel}\sin\tilde{\alpha}\,E)\left(\frac{g\beta}{2} - \frac{1}{\beta}\right). \tag{17}$$

With the orbit confined to a plane, any precession occurs about the normal to the plane, conserving $\tilde{s}_y$. Since the magnitude of $\tilde{\mathbf{s}}$ is conserved it follows that the magnitude $\tilde{s}_{\parallel}$ is also conserved. This allows $\tilde{s}_{\parallel}$ to be treated as constant in Eq. (17). Then Eq. (17) reduces to

$$\frac{d\tilde{\alpha}}{dt} = \frac{eE}{m_p c}\left(\frac{g\beta}{2} - \frac{1}{\beta}\right). \tag{18}$$

This is undoubtedly a fairly good approximate equation in any more-or-less constant electric field, but it is *exact only for the $m = 1$ Keplerian electric field*, which is the only field in which arbitrary orbits stay in a fixed plane. In fact, the derivation is not quite valid even for our $m = 1$ case. Though the design orbit is circular, the betatron orbits are slightly elliptic. This violates our assumption that orbit and electric field are orthogonal. Neglecting this amounts to dropping a term from the RHS of Eq. (16) that is down by four orders of magnitude. Furthermore this term would average to zero except for a possible non-zero commutation precession which would be expected to be down by another four orders of magnitude.

Meanwhile the velocity vector itself has precessed by angle ϑ relative to a direction fixed in the laboratory. Note that this angle ϑ, the angle of the individual particle's orbit is approximately, but not exactly equal to the angle θ of the design orbit.

In the ETEAPOT treatment each particle in an electric bend element evolves in its own plane. $\tilde{\mathbf{s}}_{\parallel}$ is the component in this plane of the total spin vector. At every entrance to an electic bend $\tilde{\mathbf{s}}_{\parallel}$ has to be calculated from the known laboratory frame description of $\mathbf{s}$, which also has to be updated as the particle exits the bend. (Ideally, in an EDM storage ring experiment any out-of-plane component of $\mathbf{s}$ would be evidence of non-vanishing electric dipole moment.)

The precession rate of ϑ is governed by the equation

$$\frac{d\vartheta}{dt} = \frac{d}{dt}\left(\frac{s}{r}\right) = \frac{eE}{p}. \tag{19}$$

where the curvature is $1/r = eE/(vp)$ and (just in this equation) s temporarily stands for arc length along the orbit. Dividing Eq. (18) by Eq. (19) and using $pc = m_p c^2 \gamma\beta$,

$$\boxed{\frac{d\tilde{\alpha}}{d\theta} = \left(\frac{g}{2} - 1\right)\gamma - \frac{g/2}{\gamma}.} \tag{20}$$

In this step we have also surrepticiously made the replacement $\vartheta \to \theta$. Even though these angles are not the same, over arbitrarily long times they advance at the same rate. In any case the error in equating ϑ to θ becomes progressively more valid in the fine-slicing limit, as the orbit is more nearly approximated by straight line segments. Explicitly the bend frame precession advance is the sum of two definite integrals

$$\widetilde{\Delta\alpha} = \left(\frac{g}{2} - 1\right) I_\gamma - \frac{g}{2} I_{\gamma i}, \tag{21}$$

where

$$I_\gamma = \int_0^\theta \gamma(\theta')d\theta', \quad \text{and} \quad I_{\gamma i} = \int_0^\theta \frac{d\theta'}{\gamma(\theta')}. \tag{22}$$

To account for fringe fields two more terms, $\widetilde{\Delta\alpha}^{\rm FF,in}$ and $\widetilde{\Delta\alpha}^{\rm FF,out}$, will later be added directly to the right hand side of Eq. (21).

A.3.2 Non-Perturbative Evaluation of the Spin Precession

Eq. (20) is susceptible to solution by an approach just like that used in the time of flight determination. The main step is to express γ as a function of θ';

$$\begin{aligned}\gamma(\theta') &= \frac{\mathcal{E}/e}{m_p c^2/e} - \frac{E_0 r_0}{m_p c^2/e}\left(\xi_{\rm co} + (\xi_{\rm in} - \xi_{\rm co})\cos Q\theta' + \frac{\xi'_{\rm in}}{Q}\sin Q\theta'\right) \\ &\equiv a + b\cos Q\theta' + c\sin Q\theta'. \end{aligned} \tag{23}$$

After this replacement, θ' is the only variable factor on the RHS of Eq. (20). All of the integrals can be evaluated in closed form. The more complicated integral is given by

$$I_{\gamma i}(\theta)Q = Q\int_0^\theta \frac{d\theta'}{a + b\cos Q\theta' + c\sin Q\theta'}. \tag{24}$$

A prescription for evaluating such integrals is given, for example, in Dwight[11], formula 456.2. Define $r = \sqrt{b^2 + c^2}$, $\sin\psi = b/r$, and $\cos\psi = \pm c/r$. (In the code one must use ψ =arctan2$(b, \pm c)$ to obtain ψ, to handle the $r = 0$ possibility.) The reason for the introduction of th $\pm$ option is explained below; until then assume the + option has been chosen. The indefinite integral is transformed to

$$\int \frac{d(Q\theta' + \psi)}{a + r\sin(Q\theta' + \psi)}. \tag{25}$$

Then, defining $x' = Q\theta' + \psi$, one obtains

$$I_{\gamma i}(\theta)Q = \int_\psi^{\psi + Q\theta} \frac{dx'}{a + r\sin x'}. \tag{26}$$

The form of this integral, as given in Dwight 436.00, depends on the relative magnitudes or a and r. In our storage ring application the oscillating part of γ is always miniscule compared to its nominal value. As a result $|a| >> |r|$ and the result is

$$I_{\gamma i}(\theta)Q = \left[\frac{2}{\sqrt{a^2-r^2}}\arctan\Big(\frac{a\tan x'/2 + r}{\sqrt{a^2-r^2}}\Big)\right]_{\psi}^{\psi+Q\theta}. \tag{27}$$

In this case the denominator of the arctan argument cannot vanish. Also, practical bend element bend angles satisfy $\theta << \pi/2$ and the arctan evaluation is unambiguous. For realistically short bend elements the $\widetilde{\Delta\alpha}$ increment cannot exceed a few percent.

Another hazard to be faced is the possibility for the upper and lower limits in Eq. (27) to be on opposite sides of a discontinuity in the arctan function. This was the motivation for introducing the $\pm$ option. Switching the initial choice from $+$ to $-$ is equivalent to switching the sign of ψ. The $\psi = 0$ possibility can be ignored since, in that case, there would be no possibility of upper and lower limits straddling the discontinuity. Switching the sign of ψ therefore gives two independent choices of upper and lower limits in Eq. (27) and, therefore, two evaluations of the definite integral, of which at most one is incorrect. It is not hard to decide which determination to discard. It has already been stated that the $\widetilde{\Delta\alpha}$ increment cannot exceed a few percent. Numerically this test has proved to be sufficient in numerous cases. But, as a further check, a perturbative evaluation, not subject to the arc tangent ambiguity, is described in the next section. The perturbative evaluation always agrees with the (correct) non-perturbative evaluation to 1/10 percent accuracy.

It has been stated that practical bend elements bend at most through a few degrees. The ETEAPOT code has no such constraint, however. The `sxf` file could, for example, represent a single inverse square law electric field of total bend angle arbitrarily larger than 2π. Though impractical for a storage ring, the resulting evolution can be (and has been) checked against celestial mechanics evaluations, such as those of Muñoz. The precautions described in the previous paragraph have to be altered for this case.

It is important not to apply any magnitude test to the accumulated precession angle $\tilde{\alpha}$, because its magnitude can become arbitrarily large over long times.

A.3.3 Perturbative Treatment Relative to the Magic Condition

In an EDM storage ring, the design γ value is set equal to the "magic" value γ_0. This suggests using the difference $\gamma - \gamma_0$ as independent variable for purposes of energy expansions. In practice this is likely to lead to confusion when, intentionally or unintentionally, the design value γ_D is not quite equal to γ_0. If a "magic" (in its physics sense) value is hard-coded then it becomes "magic" (in the computer science sense); which is something to be avoided. To avoid this we define, instead, with "D" standing for "design",

$$\Delta\gamma = \gamma - \gamma_D, \tag{28}$$

planning, usually, to identify γ_D with γ_0. Any particular particle being tracked will typically have a γ value different from both the magic value γ_0 and the design value γ_D. With $\gamma_D = \gamma_0$, one can check that $d\tilde{\alpha}/d\theta$ vanishes at the magic condition $\gamma = \gamma_0$;

$$\Big(\frac{g}{2} - 1\Big)\gamma_D - \frac{g/2}{\gamma_D} = 0. \tag{29}$$

where $a \equiv G = 1.7928474$, $g = 2G + 2 = 5.5856948$. The "magic" relativistic factor is $\gamma_0 = \sqrt{g/(g-2)} = 1.2481073$. Exploiting this relation, substituting from Eq. (28), and expanding in powers of $\Delta\gamma$,

$$\begin{aligned}\frac{d\tilde{\alpha}}{d\theta} &= \Big(\frac{g}{2} - 1\Big)(\gamma_d + \Delta\gamma) - \frac{g/(2\gamma_d)}{1 + \delta\gamma/\gamma_d} \\ &= \Big(\frac{g}{2} - 1\Big)\Delta\gamma + \frac{g}{2\gamma_D}\Big(\frac{\Delta\gamma}{\gamma_D} - \frac{\Delta\gamma^2}{\gamma_D^2} + \frac{\Delta\gamma^3}{\gamma_D^3} - \dots\Big).\end{aligned} \tag{30}$$

The infinite series in Eq. (30) would be slowly convergent except for the fact that, typically, in an storage ring, $\Delta\gamma/\gamma_0 < 10^{-3}$. So the expansion can be applied to an arbitrary accelerator and not just a frozen spin accelerator. Furthermore, at little computational cost, the series can be truncated with no numerical test nor defined tolerance, just by retaining a conservatively large number of terms.

From initial displacements $(x_{\rm in}, x'_{\rm in})$ one introduces intermediate variables,

$$\xi_{\rm in} = \frac{x_{\rm in}}{r_0 + x_{\rm in}}, \quad \xi'_{\rm in} = \frac{r_0^2 x'_{\rm in}}{(r_0 + x_{\rm in})^2}. \tag{31}$$

In terms of these variables, neglecting the $\xi_{\rm co}$ offset, evolution through a Muñoz-Pavic bend from $\theta = 0$ to θ can be approximated by

$$\begin{aligned}\frac{\Delta\gamma(\theta)}{\gamma_D} &= \frac{\mathcal{E}}{m_p c^2 \gamma_D} - 1 - \frac{eE_0 r_0}{m_p c^2 \gamma_D}\left(\cos(Q\theta)\,\xi_{\rm in} + \frac{\sin(Q\theta)}{Q}\,\xi'_{\rm in}\right) \\ &= \frac{\Delta\gamma}{\gamma_D} + \frac{eE_0 r_0 \xi_{\rm in}}{m_p c^2 \gamma_D} - \frac{eE_0 r_0}{m_p c^2 \gamma_D}\left(\cos(Q\theta)\,\xi_{\rm in} + \frac{\sin(Q\theta)}{Q}\,\xi'_{\rm in}\right)\end{aligned} \tag{32}$$

Substituting from Eq. (31) into Eq. (30) one finds, to a lowest approximation, and continuing to assume $\gamma_D = \gamma_0$,

$$\begin{aligned}\frac{d\tilde{\alpha}}{d\theta} &\approx \left(\frac{g}{2} - 1\right)\Delta\gamma + \frac{g}{2\gamma_D}\left(\frac{\Delta\gamma}{\gamma_D}\right) \\ &= \left(\frac{g}{2} - 1\right)\Delta\gamma + \frac{g}{2\gamma_D}\left(\frac{\Delta\gamma}{\gamma_D} + \frac{eE_0 r_0 \xi_{\rm in}}{m_p c^2 \gamma_D} - \frac{eE_0 r_0}{m_p c^2 \gamma_D}\left(\cos(Q\theta)\,\xi_{\rm in} + \frac{\sin(Q\theta)}{Q}\,\xi'_{\rm in}\right)\right) \\ &= \left(\frac{g}{2} - 1\right)\Delta\gamma + \frac{g}{2\gamma_D}\left(\frac{\Delta\gamma}{\gamma_D} + \frac{eE_0 r_0}{m_p c^2 \gamma_D}\left(\big(1 - \cos(Q\theta)\big)\,\xi_{\rm in} - \frac{\sin(Q\theta)}{Q}\,\xi'_{\rm in}\right)\right).\end{aligned} \tag{33}$$

This can be trivially integrated to give $\widetilde{\Delta\alpha}$. The total energy $\mathcal{E}$, is a constant of the motion (not counting RF cavities). If needed, higher order terms can be included similarly.

The phase advance over any single Muñoz-Pavic bend will normally be very small compared to 2π and the oscillating factor can have either sign. In fact the phase advances may sometimes be sufficiently small across individual bends to legitimize approximating $\cos Q\theta \approx 1$ and $\sin(Q\theta) \approx Q\theta$ to give a quick "ball park" estimate of the spin precession.

The way vertical betatron oscillations are treated in ETEAPOT, is to regard the Muñoz-Pavic plane as being slightly tilted. This is why the result in Eq. (33) has been expressed as $\widetilde{\Delta\alpha}$. As explained previously, small spin orientation corrections are required at entrance to and exit from bend elements, to consistently integrate the 3D and 2D descriptions.

A.4 Spin Evolution Through Fringe Fields

So far in ETEAPOT, as a particle enters or exits a bend element, its potential energy has been treated as changing discontinuously with its kinetic energy changing correspondingly. We now have to treat this region more carefully. Instead of treating the potential as discontinuous, we now assume the change occurs over a longitudinal distance $\Delta z^{\rm FF}$ which, for estimation purposes, we take equal to the separation distance (symbol *gap*) between the electrodes; $\Delta z = gap$. (For the "protonium" model introduced later, the drift lengths are taken to be almost zero and fringe field spin precession is negligible.) The fringe field region is assumed to be short enough to be treated as "thin". That is, any change in the particle's radial offset occuring in range Δz is to be neglected and the integrated deflection applied at the center (i.e. the edge of the bend). As a result the curve $x(z)$ is continuous, but its slope dx/dz is discontinuous. Entrance transitions from outside a bend to inside are described first.

Inside the bending element the increase in potential energy from orbit centerline to radial position x is $e\Delta V(x)$. As synchroton oscillations move the particle radially in and out, the sign of $\Delta V(x)$, just inside the bend edge oscillates between negative and positive values, and the sign of the deviation from

the magic velocity oscillates correspondingly. This will tend to average away the spin run-out occurring in the fringe field region over times long compared to the synchrotron period. In the long run it is the deviation from zero of this average that has to be determined. This can be by pure numerical tracking or theoretically or, most likely, by a theoretical averaging based on numerical tracking data.

Once one is able to determine the spin decoherence the task will shift to designing sextupole distributions capable of increasing the spin coherence time SCT. Our approach will be to study the effectiveness of such schemes before attempting to improve the precision of our fringe field treatment.

The deflection angle $\theta^{(FF)}$ of the design orbit in the fringe field at one such edge is approximately

$$\theta^{(FF)} \approx \frac{1}{2}\,\frac{\Delta z^{\rm FF}}{r_0} \quad \Big(\stackrel{\rm e.g.}{=} 0.5 \times 0.03/40 = 0.375 \times 10^{-3} \Big); \tag{34}$$

this is half of the deflection occurring in advancing a distance *gap* in the interior of the bend. (The angle $\theta^{(FF)}$ is implicitly assumed to be positive, irrespective of whether the orbit is clockwise or counter-clockwise.) Consider a particle approaching the fringe field region at radial displacement x. At the longitudinal center of the fringe field region the kinetic energy of this particle deviates from its "proper" (i.e. fully-inside value at radial displacement x) by the amount

$$\Delta\gamma^{(FF)}(x) \approx \frac{1}{2}\,\frac{\Delta V(x)}{m_p c^2/e} \approx \frac{1}{2}\,\frac{E\,x}{m_p c^2/e}, \tag{35}$$

where $\Delta V_{\rm tot}$ is the total voltage increase from inner electrode to outer electrode. (The electric field points radially inward in order for positive particles to bend toward negative x but, by convention, E is positive.) Here, for simplicity, we are neglecting the fact that the actual electric field will have more complicated x-dependence depending, for example, on the value of the field index m. Our assumed fringe field spatial dependence is also simplistic.

According to Eq. (30) the leading effect of passage through a bend region with γ deviation from magic $\Delta\gamma$, is a rate of change of spin angle α per unit deflection angle θ given by

$$\frac{d\alpha}{d\theta} \approx \left(\frac{g}{2} - 1 + \frac{g/2}{\gamma_0^2}\right)\Delta\gamma \quad \Big(\stackrel{\rm for\ proton}{=} 3.586\,\Delta\gamma. \Big) \tag{36}$$

Combining equations, the excess angular advance occurring while entering the bend at displacement x is

$$\boxed{\widetilde{\Delta\alpha}^{\rm FF} = +\left(\frac{g}{2} - 1 + \frac{g/2}{\gamma_0^2}\right)\frac{1}{2}\,\frac{E\,x}{m_p c^2/e}\,\frac{1}{2}\,\frac{\Delta z^{\rm FF}}{r_0}.} \tag{37}$$

(**Aside:** it may be appropriate to keep another term in expansion (36) in order to include the effect that dispersion introduces a correlation between γ and x which, after averaging, leaves a finite precession, even if $< x >$ vanishes in Eq. (37) .)

In our initial treatment of this edge effect we are assuming this precession lies in exactly the same plane as the orbit plane of the particle in the bend element, justifying the notation $\widetilde{\Delta\alpha}^{\rm FF}$ Entrance (and, later, exit) values can simply be added to the main precession through the bend element. Meanwhile, in the fringe field region the advance of the tangent to the orbit is $\theta^{(FF)}$ as given by Eq. (34). The + sign on the rhs of Eq. (37) reflects the fact that, for a particle displaced radially outward, the particle momentum is completing some of its rotation in the fringe field where its magnitude is more positive than in the bend interior.

Though the fringe field precession occurs continuously over the range *gap* it is applied discontinuously at the bend edge. This is consistent with our hard edge treatment of the particle's momentum evolution. Because $\widetilde{\alpha}$ is measured relative to the orbit direction, Eq. (37) gives the spin angle precession over and above the advance of the tangent to the orbit.

The fact that spin and momentum angular advances do not match has come about because the particle has bent appreciably while its speed deviates from the magic value. On exiting the bend element the particle also bends appreciably while its γ deviation is given by the same formula (35). Eq. (37) therefore

applies to both entrance and exit. Unfortunately this means that excess input precession and excess output precession combine constructively rather than tending to cancel (as edge focusing sometimes does.)

The largest magnitude $\Delta\gamma^{(FF)}$ can have is

$$|\Delta\gamma^{(FF)}_{\max}| = \frac{1}{4}\,\frac{E\,gap}{m_p c^2/e} \quad \left(\stackrel{\text{e.g.}}{=} \frac{1}{4}\,\frac{(10.5\times10^6)\times 0.03}{0.938\times10^9} = 0.84\times10^{-4}.\right) \tag{38}$$

For a particle with magic velocity skimming the outer electrode, where the effect is maximum, the angular runout is given by

$$\begin{aligned} |\Delta\alpha^{(FF)}_{\max}| &\approx \left(\frac{g}{2} - 1 + \frac{g/2}{\gamma_0^2}\right)\Delta\gamma_{\max}\,\Delta\theta^{(FF)} \\ &= 3.586\times(0.84\times10^{-4})\times(0.375\times10^{-3}) \\ &= 1.13\times10^{-7}\,\text{radians/edge}. \end{aligned} \tag{39}$$

With perhaps 50 edges in the lattice, and revolution frequency of about 1 MHz, the maximum spin runout will be about one revolution per second. This vastly exaggerates the spin decoherence, of course, because it does not account for the averaging effect of synchrotron oscillations. A challenge for lattice design is to perfect the synchrotron oscillation averaging to zero.

A.5 Spin Evolution Through Thin Elements

In ETEAPOT the only "thick" elements are bends. Spin evolution through them has already been discussed. All other elements are treated as thin element kicks. Rearranging Eq. (36) produces, for spin evolution through a thin element,

$$\boxed{|\widetilde{\Delta\alpha}| \approx \left(\frac{g}{2} - 1 + \frac{g/2}{\gamma_0^2}\right)\Delta\gamma\,\widetilde{\Delta\theta}} \tag{40}$$

where $\widetilde{\Delta\theta}$ is positive by definition and $\widetilde{\Delta\alpha}$ is the angular deviation of the bend plane spin coordinate relative to the orbit. The absolute value sign in this equation eventually has to be removed; it is included here so that the discussion of signs can be deferred. In paraxial approximation, for a particle with transverse position (x, y), the magnitude of the (not necessarily horizontal) angular deviation $\widetilde{\Delta\theta}$ in a quadrupole of strength q is given by

$$\widetilde{\Delta\theta} = |q|\sqrt{x^2+y^2}, \tag{41}$$

where q is the inverse focal length of the quadrupole. (The magnitude of the angular deflections in sextupoles and higher order multipoles are also functions only of the combination $\sqrt{x^2+y^2}$).

A significant complication concerns the sign of the $\widetilde{\Delta\alpha}$. For a *horizontally focusing or defocusing quadrupole* there is no ambiguity, since the bend plane in the quadrupole is the same as the overall (horizontal) lattice design plane. In this case, with $y = 0$, Eq. (40) can be made more explicit;

$$\widetilde{\Delta\alpha}_h \approx \left(\frac{g}{2} - 1 + \frac{g/2}{\gamma_0^2}\right)\Delta\gamma\,q\,x. \tag{42}$$

where, by convention, a horizontal *focusing* quad has $q > 0$. The sign in Eq. (42) reflects the fact that, for $x > 0$ and $q > 0$, the quadrupole "helps" by bending the momentum in the same sense as the bending elements. This formula makes it clear that reversing the sign of q reverses the sign of $\widetilde{\Delta\alpha}$.

For obtaining the proper sign for vertically focusing quadrupoles it is necessary to handle consistently the transformation from laboratory to bend frame spin coordinates, which is why the sign issue has been deferred until after discussing this transformation.

Most of the elements in a storage ring cause spin precession which approximately conserves the vertical component of spin $s_y\hat{\mathbf{y}}$. The leading exceptions to this in a proton EDM storage rings are the vertically

focusing or defocusing quadrupoles present in the lattice to keep β_x magnageably small. Particles having non-vanishing vertical betatron amplitude are deflected vertically which causes $s_y\hat{\mathbf{y}}$ to precess. (As an aside it can be mentioned that there is a very strong tendency for this precession to cancel in subsequent quadrupoles and, therefore, probably not contribute significantly to spin decoherence. Nevertheless it is important for the precession to be modeled correctly.) All quadrupoles and sextupoles in the lattice cause similar precession to at least some degree.

The planes of deflection for particles incident on a quadrupole are shown in Figure 7. In a perfect multipole field the magnitude of the total deflection angle is constant on a contour of fixed radius (i.e. a circle centered on the origin.) For a particle incident at (x_0, y_0) the equation of the line of intersection of the deflection plane with the transverse plane is

$$y = y_0 - \frac{y_0}{x_0}(y - y_0), \tag{43}$$

As shown if the figure, the roll-angle of the deflection plane (with counter-clockwise roll taken as positive) is $\phi = \tan^{-1}(y_0/x_0)$, irrespective of quadrant and whether the quadrupole is focusing or defocusing. However the inverse tangent function is, itself, multiple valued. To make it single valued one can determine ϕ using

$$\phi = \text{arctan2}(qy_0, qx_0). \tag{44}$$

Along with Eq. (40), this establishes both the sign and magnitude of $\widetilde{\Delta\alpha}$, while preserving the sign reversal when the sign of q reverses. This should be checked numerically in all quadrants. Substitution

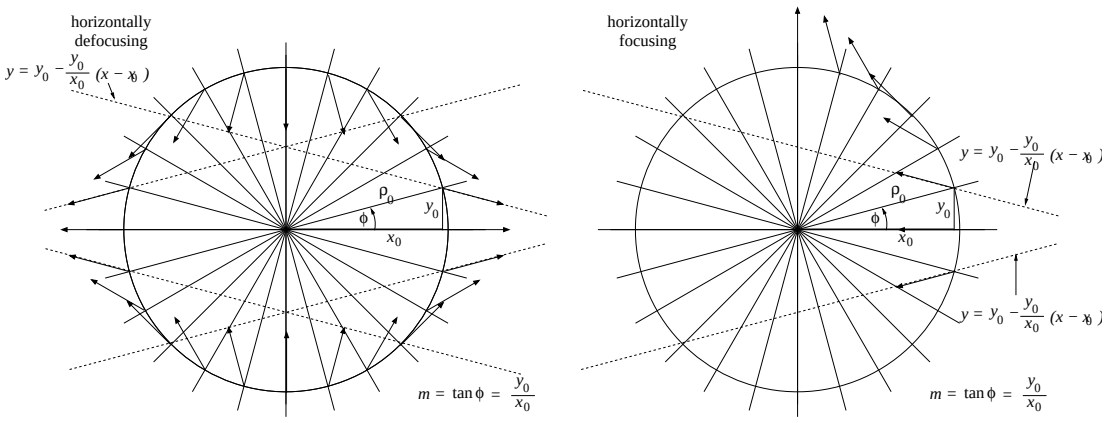

Figure 7: The broken lines shows the deflection planes for particle with dispacements x_0, y_0 in various quadrants, incident on an erect quadrupole. The roll-angle of the deflection plane (with counter-clockwise roll taken as positive) is $\phi = \tan^{-1}(y_0/x_0)$ irrespective of quadrant, and irrespective of whether the quadrupole is focusing or defocusing.

into Eq. (14) and defining $\rho_0 = \sqrt{x_0^2 + y_0^2}$, produces

$$\begin{pmatrix} s_x'' \\ s_y'' \\ s_z'' \end{pmatrix} = \begin{pmatrix} \cos\phi & -\sin\phi & 0 \\ \sin\phi & \cos\phi & 0 \\ 0 & 0 & 1 \end{pmatrix} \begin{pmatrix} \cos\widetilde{\Delta\alpha} & 0 & -\sin\widetilde{\Delta\alpha} \\ 0 & 1 & 0 \\ \sin\widetilde{\Delta\alpha} & 0 & \cos\widetilde{\Delta\alpha} \end{pmatrix} \begin{pmatrix} \cos\phi & \sin\phi & 0 \\ -\sin\phi & \cos\phi & 0 \\ 0 & 0 & 1 \end{pmatrix} \begin{pmatrix} s_x \\ s_y \\ s_z \end{pmatrix} \tag{45}$$

It is appropriate, to improve numerical precision, to break the central matrix into two terms, $\mathbf{I}+\mathbf{\Delta}$ where $\mathbf{I}$ is the identity matrix and $\mathbf{\Delta}$ is a small deviation. Then, since $\mathbf{I}$ commutes with the outer matrices, and

their product is $\mathbf{I}$, the final result is equal to $\mathbf{I}$ plus a small deviation. The matrix product is

$$\begin{pmatrix} \cos\phi & -\sin\phi & 0 \\ \sin\phi & \cos\phi & 0 \\ 0 & 0 & 1 \end{pmatrix} \left(\begin{pmatrix} 1 & 0 & 0 \\ 0 & 1 & 0 \\ 0 & 0 & 1 \end{pmatrix} + 2\sin(\widetilde{\Delta\alpha}/2) \begin{pmatrix} -\sin\widetilde{\Delta\alpha}/2 & 0 & -\cos\widetilde{\Delta\alpha}/2 \\ 0 & 1 & 0 \\ \cos\widetilde{\Delta\alpha}/2 & 0 & -\sin\widetilde{\Delta\alpha}/2 \end{pmatrix} \right) \begin{pmatrix} \cos\phi & \sin\phi & 0 \\ -\sin\phi & \cos\phi & 0 \\ 0 & 0 & 1 \end{pmatrix}$$
$$= \begin{pmatrix} 1 & 0 & 0 \\ 0 & 1 & 0 \\ 0 & 0 & 1 \end{pmatrix} + 2\sin(\widetilde{\Delta\alpha}/2) \begin{pmatrix} \cos\phi & -\sin\phi & 0 \\ \sin\phi & \cos\phi & 0 \\ 0 & 0 & 1 \end{pmatrix} \begin{pmatrix} -\sin\widetilde{\Delta\alpha}/2 & 0 & -\cos\widetilde{\Delta\alpha}/2 \\ 0 & 1 & 0 \\ \cos\widetilde{\Delta\alpha}/2 & 0 & -\sin\widetilde{\Delta\alpha}/2 \end{pmatrix} \begin{pmatrix} \cos\phi & \sin\phi & 0 \\ -\sin\phi & \cos\phi & 0 \\ 0 & 0 & 1 \end{pmatrix}. \tag{46}$$

Calculation of the *changes* in spin coordinates requires only the second term, which is

$$2\sin(\widetilde{\Delta\alpha}/2) \begin{pmatrix} -\cos(\phi)^2\sin(\widetilde{\Delta\alpha}/2) & -\cos(\phi)\sin(\widetilde{\Delta\alpha}/2)\sin(\phi) & -\cos(\phi)\cos(\widetilde{\Delta\alpha}/2) \\ -\cos(\phi)\sin(\widetilde{\Delta\alpha}/2)\sin(\phi) & -\sin(\phi)^2\sin(\widetilde{\Delta\alpha}/2) & -\sin(\phi)\cos(\widetilde{\Delta\alpha}/2) \\ \cos(\phi)\cos(\widetilde{\Delta\alpha}/2) & \sin(\phi)\cos(\widetilde{\Delta\alpha}/2) & -\sin(\widetilde{\Delta\alpha}/2) \end{pmatrix}. \tag{47}$$

As mentioned before, all components in this matrix are small, of order $\widetilde{\Delta\alpha}$ or smaller, even if the angle ϕ is as great as $\pi/2$. Multiplying this matrix on the right by $(s_x, s_y, s_z)^T$ produces deviations $(\Delta s_x, \Delta s_y, \Delta s_z)$ which, added to (s_x, s_y, s_z), give the output spin coordinates.

A.6 Formulas Sensitive to Precession Sense

Hardly anything can be more confusing than what constitutes positive sense of precession of momentum and spin, especially in a storage ring in which there are both CW and CCW beam directions. One can haggle whether or not the sign choices in Fig. (6) were chosen advisedly. But, for better or worse, we define the sense of momentum precession in that figure to be *positive*. We also define the vertical axis to be always the same, and specified by the unit vector $\hat{\mathbf{y}}$.

In electric bending elements, for momenta close to the magic momentum the rates of precession of spin and momentum are approximately equal, which makes it easy to establish the signs of contributions to the spin precession. The same was true, in Eq. (42), for horizontally focusing quads. But for vertically focusing quads, and multipoles in general it seems advisable to develop an algebraic test, based on dot products and cross products of vectors, in order to specify precession senses.

The sense of momentum precession in Fig. (6), which we have defined to be positive, can also be defined to be the sign of the scalar product

$$\Big(\frac{d\mathbf{p}}{dt} \times \mathbf{p}\Big) \cdot \hat{\mathbf{y}} > 0. \tag{48}$$

with the momentum $\mathbf{p}$ always lying approximately in the horizontal plane, which is normal to $\hat{\mathbf{y}}$. When expressed in terms of the electric field using Newton's law, the same condition for positive sense precession can be expressed

$$e\Big(\mathbf{E} \times \mathbf{p}\Big) \cdot \hat{\mathbf{y}} > 0, \tag{49}$$

with $\mathbf{E}$ also approximately horizontal.

Similarly, the positive sense for spin precession can be defined by

$$\Big(\frac{d\mathbf{s}}{dt} \times \mathbf{s}\Big) \cdot \hat{\mathbf{y}} > 0. \tag{50}$$

Using Jackson's Eq. (11.170), the spin precession in electric field $\mathbf{E}$ is given by

$$\frac{d\mathbf{s}}{dt} = -\frac{e}{m^2c^2\gamma}\,\mathbf{s} \times (\frac{g}{2} - \frac{\gamma}{\gamma+1})(\mathbf{p} \times \mathbf{E}) \tag{51}$$

Substituting this expression into Eq. (50) produces

$$-\frac{e}{m^2c^2\gamma}\,(\frac{g}{2}-\frac{\gamma}{\gamma+1})\Big(\Big(\mathbf{s}\times(\mathbf{p}\times\mathbf{E})\Big)\times\mathbf{s}\Big)\cdot\hat{\mathbf{y}}>0. \tag{52}$$

Simplifying the triple cross product and using the fact that $\mathbf{s}$ is a unit vector, this reduces to

$$\frac{e}{m^2c^2\gamma}\,(\frac{g}{2}-\frac{\gamma}{\gamma+1})\Big(\Big(-\mathbf{s}\cdot(\mathbf{E}\times\mathbf{p})\Big)\mathbf{s}+\mathbf{E}\times\mathbf{p}\Big)\cdot\hat{\mathbf{y}}>0. \tag{53}$$

For any spin vector $\mathbf{s}$ lying in the plane perpendicular to $\mathbf{E}\times\mathbf{p}$ (which, in the pEDM experiment is always approximately parallel to the y-axis) the condition reduces to

$$\frac{e}{m^2c^2\gamma}\,(\frac{g}{2}-\frac{\gamma}{\gamma+1})\,\mathbf{E}\times\mathbf{p}\cdot\hat{\mathbf{y}}>0. \tag{54}$$

B UAL/ETEAPOT Code Description

B.1 Server/Client Architecture

B.2 User Responsibility in Connection with "User Manifest"

B.2.1 User Manifest File Contents

There are two major factors that make the unambiguous definition of parameters more difficult in ETEAPOT than in TEAPOT (or any other accelerator simulation code, such as MAD, designed primarily to simulate magnetic storage rings). The traditional accelerator physics transfer matrix formalism "geometricizes" the lattice; that is, bend elements are fully described by lengths and bend angles, quadrupoles by focal lengths, and beams by design momentum and fractional offsets. Only in RF cavities do particle energies change, and these changes are immediately converted to changes in momentum magnitudes. In this geometricized formalism, like the geometric optics formalism, determination of spatial orbits is paramount, evolution of position as a function of time can either be ignored, or determined by post processing. In this formalism, the spatial orbits can be determined from the `.sxf` lattice description file. It is unnecessary for the user to provide more than a very small number of extra parameters, such as particle charge, to complete the parameterization of the system to be simulated.

In an electric ring, changes in potential energy are constantly being reflected in changes in velocity and magnitude of momentum. The unambiguous parameterization of the system to be simulated requires all dynamical beam quantities to be established from the beginning.

Initiallizing the parameterization of the spins is the other essential complication in applying ETEAPOT to, for example, a simulation of spin evolution in a storage ring to be used to measure the proton EDM.

```
\subsubsection{extractParameters.h}
   std::string sxfFile = argv[1];
// std::string sxfFile = "./data/";
// sxfFile += argv[2];
// sxfFile += ".sxf";

 std::string outputFile = "./out/cpp/";
 outputFile += mysxfbase;
 outputFile += ".sxf";
 std::string mapFile = "./out/cpp/";
 mapFile += mysxfbase;
 mapFile += ".map1";
 std::string twissFile = "./out/cpp/";
 twissFile += mysxfbase;
```

```
 twissFile += ".twiss";
//std::string apdfFile = "./data/eteapotConservedVector.apdf";
//std::string apdfFile = "./data/eteapotLegacyBenchmark.apdf";
  std::string apdfFile = "./data/eteapot.apdf";
 std::string orbitFile = "./out/cpp/";
 orbitFile += mysxfbase;
 orbitFile += ".orbit";

 int split = 1;            // old split specification
 int splitForBends = 0;    // new split specification
 int splitForQuads = 0;    // new split specification
 int splitForSexts = 0;    // new split specification
 int order = 2;
 int turns;                // specified as 1 in trtrin (for post processing)
                           // might be overwritten tp multiple turns (e.g. 10) in simulatedProbeValues


\subsubsection{designBeamValues.hh}
//#define GAMMA_FROZEN_SPIN 1.24810735
#define INJECTION_AMBIT   argv[3]

std::cout     << "#################################   Design Beam Orientation\n";
  double gamma0  = UAL::pFSG;                      // fundamental kinematic parameter
//double gamma0  = GAMMA_FROZEN_SPIN;              // fundamental kinematic parameter
double c       = 1.;                               // other units (mks) have 2.99792458e8 m/s
double b0      = sqrt(1.-1./gamma0/gamma0);        // equivalent fundamental kinematic parameter
double v0      = b0*c;                             // equivalent fundamental kinematic parameter

// \$UAL/codes/PAC/src/PAC/Beam/BeamAttributes.hh   // # (index) of member variable
double m0      = UAL::pmass;                       // 2
double e0      = gamma0*m0;                        // 1
double p0      = gamma0*m0*v0;                     //

// double q0      = UAL::elemCharge;               // 3
double q0      = 1.0;                              // 3
double t0      = 0.;                               // 4
// double f0      = 1;                             // 5
double f0      = 541426.7816;                      // 5
double M0      = 1.;                               // 6
double G0      = UAL::pG;                          // 7
double g0      = UAL::pg;                          // 7
double IA      = atof(INJECTION_AMBIT);            // (10) not used
double L0      = IA*p0;                            // 8
double El0     = +1.048270839000000e+07;//10.5e6;  // 9

std::cout     << "#################################   Design Beam Orientation\n";



\subsubsection{simulatedProbeValues}
//#include "probeDataForTwiss"

double k       = IA*p0*v0;                         //
```

```
//                   probe deviations
double  dx     = 0.01;   //   +x1typ;
double  dy     = 0.0;
double  dz     = 0.0;

double dpx     = 0.0;
double dpy     = 0.0;
double dpz     = 0.0;

double dt      = 0.0;
//                   probe deviations

double rin     = IA+dx;                              //
double rinEx   = sqrt((IA+dx)*(IA+dx)+dy*dy+dz*dz);//
  double gamma = (k/rinEx-k/IA)/m0/c/c;              //
         gamma = gamma+gamma0;
//double gamma   = gamma0;                           //
double Ein     = gamma*m0*c*c-k/rinEx;               // E for compatibility with Munoz

double Edes    = m0*c*c/gamma0;                      // Design Energy (Munoz potential)
double dE      = 0.000041;//0.00014954888;   //   Ein-Edes;

double dpxbyp0 = dpx/p0;
double dpybyp0 = dpy/p0;
double dEbyp0  = dE /p0;

//#include "trtrin"

//         This configuration is for a standard one turn bunch for post processing.
//     Uncomment this next line to look at multi turns for your particle specified above.
//turns=10;
  bunch[ 0].getPosition().set(     dx,dpxbyp0,     dy,dpybyp0,     dt, dEbyp0 );

#include "printProbeValues"



\subsubsection{userBunch}
PAC::Bunch bunch(21);                                 // bunch with 21 particle(s)
PAC::Spin * spinX   = new PAC::Spin[21];              // the corresponding spins
bunch.setBeamAttributes(ba);

bunch[ 1].getPosition().set( +x1typ,       0,      0,      0,      0,      0 );
bunch[ 2].getPosition().set( -x1typ,       0,      0,      0,      0,      0 );
bunch[ 3].getPosition().set(      0,  +x2typ,      0,      0,      0,      0 );
bunch[ 4].getPosition().set(      0,  -x2typ,      0,      0,      0,      0 );
bunch[ 5].getPosition().set(      0,       0, +y1typ,      0,      0,      0 );
bunch[ 6].getPosition().set(      0,       0, -y1typ,      0,      0,      0 );
bunch[ 7].getPosition().set(      0,       0,      0, +y2typ,      0,      0 );
bunch[ 8].getPosition().set(      0,       0,      0, -y2typ,      0,      0 );
bunch[ 9].getPosition().set(      0,       0,      0,      0,      0,+deltyp );
bunch[10].getPosition().set(      0,       0,      0,      0,      0,-deltyp );
```

```
bunch[11].getPosition().set(  0.005,       0,      0,   0,      0,      0 );
bunch[12].getPosition().set( -0.005,       0,      0,   0,      0,      0 );
bunch[13].getPosition().set(   0,  0.0002,      0,   0,      0,      0 );
bunch[14].getPosition().set(      0, -0.0002,      0,      0,      0,      0 );
bunch[15].getPosition().set(     0,   0,   0.01,      0,      0,      0 );
bunch[16].getPosition().set(     0,   0,   0,  0.001,      0,      0 );
bunch[17].getPosition().set(     0,   0,      0,      0,      0, 5.85e-5 );
bunch[18].getPosition().set(     0,       0,      0,      0,      0,-5.85e-5 );
bunch[19].getPosition().set(     0,       0,      0,      0,      0,      0 );
bunch[20].getPosition().set(     0,       0,      0,      0,      0,      0 );


\subsubsection{eteapot.apdf}
<apdf>
  <propagator id="ETEAPOT_MltTurn" accelerator="ring">
     <create>
       <link algorithm="ETEAPOT_MltTurn::MarkerTracker" types="Marker"/>
       <link algorithm="ETEAPOT_MltTurn::DriftTracker" types="Drift|Default"/>
       <link algorithm="ETEAPOT_MltTurn::DipoleTracker" types="Sbend"/>
       <link algorithm="ETEAPOT_MltTurn::MltTracker" types="Quadrupole|Sextupole"/>
       <link algorithm="ETEAPOT_MltTurn::RFCavityTracker" types="RfCavity"/>
     </create>
  </propagator>
</apdf>
\subsubsection{lattice.sxf}
See earlier benchmark report\cite{BenchmarkI} for an
example ``.sxf'' lattice description file.
```

References

[1] J.D. Talman and R.M. Talman, *UAL/ETEAPOT Proton EDM Benchmark Comparisons III: Longitudinal Dynamics and Synchrotron Oscillations (Revised Version),* EDM Group report, June 1, 2014

[2] J.D. Talman and R.M. Talman, *UAL/ETEAPOT Results (Augmented) for Proton EDM Benchmark Lattices,* BNL internal report, April 29, 2012

[3] J.D. Talman and R.M. Talman, *UAL/ETEAPOT Proton EDM Benchmark Comparisons II: Transfer Matrices and Twiss Functions,* BNL internal report, August 30, 2012

[4] D. Edwards and M. Syphers, *Longitudinal Motion,* p. 53 in *Handbook of Accelerator Physics and Engineering,* editors, A. Chao and M. Tigner, World Scientific, 2002

[5] N. Malitsky, J. Talman, and R. Talman, *Appendix UALcode: Development of the UAL/ETEAPOT Code for the Proton EDM Experiment,* UAL/ETEAPOT documentation (frequently revised), August, 2012

[6] Storage Ring EDM Collaboration, *A Proposal to Measure the Proton Electric Dipole Moment with* 10^{-29} *e-cm Sensitivity,* especially Appendix 1. October, 2011

[7] R. Talman, *Reduced Dispersion Proton EDM Storage Ring Lattices,* Internal Report, 12 December, 2012

[8] M. Plotkin, *The Brookhaven Electron Analog, 1953-1957,* Brookhaven Internal Report, BNL-45058, 1991

[9] E. Forest, *Beam Dynamics, A New Attitude and Framework,* Harwood Academic Publishers, 1998. See especially Section 12.2.3,

[10] G. Muñoz and I. Pavic, *A Hamilton-like vector for the special-relativistic Coulomb problem,* Eur. J. Phys. **27**, 1007-1018, 2006

[11] H.B. Dwight, *Tables of Integrals and Other Mathematical Data,* MacMillan Publishing Co., Inc., 1961

[12] J. Jackson, *Classical Electrodynamics,* 3rd edition, John Wiley, 1998